

# SCIENTIFIC REPORTS



OPEN

## Model predictions of features in microsaccade-related neural responses in a feedforward network with short-term synaptic depression

Jian-Fang Zhou<sup>1</sup>, Wu-Jie Yuan<sup>1,2</sup>, Zhao Zhou<sup>1</sup> & Changsong Zhou<sup>2,3,4</sup>

Recently, the significant microsaccade-induced neural responses have been extensively observed in experiments. To explore the underlying mechanisms of the observed neural responses, a feedforward network model with short-term synaptic depression has been proposed [Yuan, W.-J., Dimigen, O., Sommer, W. and Zhou, C. *Front. Comput. Neurosci.* 7, 47 (2013)]. The depression model not only gave an explanation for microsaccades in counteracting visual fading, but also successfully reproduced several microsaccade-related features in experimental findings. These results strongly suggest that, the depression model is very useful to investigate microsaccade-related neural responses. In this paper, by using the model, we extensively study and predict the dependence of microsaccade-related neural responses on several key parameters, which could be tuned in experiments. Particularly, we provide a significant prediction that microsaccade-related neural response also complies with the property “sharper is better” observed in many contexts in neuroscience. Importantly, the property exhibits a power-law relationship between the width of input signal and the responsive effectiveness, which is robust against many parameters in the model. By using mean field theory, we analytically investigate the robust power-law property. Our predictions would give theoretical guidance for further experimental investigations of the functional role of microsaccades in visual information processing.

Microsaccades are the involuntary, fast, and very small eye movements that occur during visual fixation. Over the past decade, the behavioral properties and functional role of microsaccades have been widely investigated<sup>1–13</sup>. It has been found that microsaccades play an important functional role in counteracting visual fading. In order to study neural dynamical mechanism of microsaccades for counteracting perceptual fading, neural responses correlated with microsaccades have been extensively studied in experiments at different levels—from neuronal activities<sup>7,11,14,15</sup> to electroencephalogram (EEG)<sup>9,16</sup> and functional magnetic resonance imaging (fMRI)<sup>5,12</sup>—in a number of cortical areas involved in visual information processing, including V1<sup>5,7,12</sup>, V2<sup>5,12,14</sup>, V3<sup>12</sup>, V4<sup>14</sup>, and MT<sup>12,15</sup>.

Recently, a report gave an explanation for microsaccades in counteracting visual fading by constructing a feedforward network model with short-term depression (STD) at thalamocortical synapses<sup>17</sup>, alternative to the assumption of retinal adaptation. The adapted synapses subjected to STD led to response depression in V1, which induces visual fading because of sustained depression during fixation. Therefore, it is possible that the generation of microsaccades serves to counteract the STD-induced depression of neuronal activity in order to counteract visual fading. In particular, the depressed model successfully reproduced several microsaccade-related

<sup>1</sup>College of Physics and Electronic Information, Huaibei Normal University, Huaibei 235000, China. <sup>2</sup>Department of Physics, Centre for Nonlinear Studies and the Beijing-Hong Kong-Singapore Joint Centre for Nonlinear and Complex Systems (Hong Kong), Institute of Computational and Theoretical Studies, Hong Kong Baptist University, Kowloon Tong, Hong Kong. <sup>3</sup>Beijing Computational Science Research Center, Beijing 100084, China. <sup>4</sup>Research Centre, HKBU Institute of Research and Continuing Education, Virtual University Park Building, South Area Hi-tech Industrial Park, Shenzhen, China. Correspondence and requests for materials should be addressed to W.-J.Y. (email: yuanwj2005@163.com) or C.Z. (email: cszhou@hkbu.edu.hk)

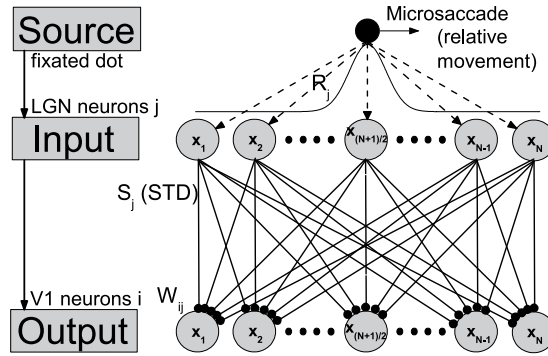


**Figure 1. (Adapted from Ref. 17) The feedforward network model including STD during fixation with microsaccade.** Here, neurons in LGN and V1 are labeled and arranged by the center positions  $x_j$  and  $x_i$  of their receptive fields in the ranges from  $-L$  to  $L$ , respectively. Gaussian filters (receptive fields) in LGN layer transform the afferent stimuli evoked by fixated dot into the inputs with Gaussian firing rate profile:  $R_j = G_1(x_j) = A \exp^{-(x_j - x_{(N+1)/2})^2 / \sigma_1^2} = A \exp^{-x_j^2 / \sigma_1^2}$ . The  $A$  represents the amplitude of a visual input at fixated-dot position  $x_{(N+1)/2} = 0$ . The  $\sigma_1$  is width of the tuning curve. The output layer V1 is connected to input layer LGN by thalamocortical synapses with synaptic strengths  $S_j$ , which are subjected to the modification: STD. These connecting weights  $W_{ij}$  follow the Gaussian tuning curve:  $W_{ij} = G_2(x_j - x_i) = \exp^{-(x_j - x_i)^2 / \sigma_2^2}$ , where  $x_j - x_i$  denotes the position difference of receptive field centers between the input neuron  $j$  and the output neuron  $i$ . The microsaccade during fixation can be regarded as relative movement of the fixated dot over LGN with microsaccadic magnitude  $\Delta M$ . In order to eliminate the effect of boundary owing to the limited scale of network, the corresponding input tuning curve  $G_1$  is extended to a period function with period  $2L$ .

experimental observations. For example, the neural response after microsaccade is stronger when a rhythmically flashing stimulus bar is on during fixation, as compared to a condition in which the bar is always on (stationary, i.e., non-flashing). The response peak induced by microsaccade increases with the increasing of microsaccadic magnitude or velocity. Moreover, the increasing response reaches saturation for large microsaccadic magnitude or velocity.

It was found by model simulations, that the above results are attributed to the sensitivity of STD to the change of stimuli<sup>17</sup>. These findings strongly suggest that the depression model is very useful to investigate microsaccade-related neural responses. Indeed, computational studies have explored the effect of STD on network dynamics and found various rich dynamical behaviors<sup>18–21</sup>, suggesting many important roles of STD in neural computations. Thus, the depression model can be expected to produce other abundant features in microsaccade-related neural responses. Model predictions of such features would provide theoretical guidance for experimental investigations. In this paper, by using the model, we extensively study the features of microsaccade-related neural responses with respect to several key parameters, which could be experimentally tested in future.

### Methods

According to visual pathway<sup>22,23</sup>, a feedforward network model consisting of two layers corresponding to LGN and V1 with STD at thalamocortical synapses was proposed in Fig. 1<sup>17</sup>. Evoked by fixated dot, the LGN neuron  $j$  fires with rate  $R_j$  following Gaussian tuning curve  $G_1$  (shown in Fig. 1). Then, the firings  $R_j$  are straightly projected to V1 neuron  $i$  by STD synapses with linking weights  $W_{ij}$  following Gaussian tuning curve  $G_2$  (shown in Fig. 1). The membrane potential  $V_i$  of V1 neuron  $i$  in output layer is described by

$$\tau_m \frac{dV_i}{dt} = V_0 - V_i + \sum_{j=1}^N g W_{ij} S_j(t) (V_E - V_i) \delta(t - t_{sp}^j). \quad (1)$$

Here, we adopt the experimentally fitted parameter values  $\tau_m = 30$  ms,  $V_0 = -70$  mV and  $V_E = 0$  mV<sup>24,25</sup>. Each V1 neuron  $i$  integrates inputs coming from LGN neurons  $j$  at spike time  $t_{sp}^j$  distributed as Poisson spike trains  $R_j$  by chemical couplings of  $\delta$  function. When  $V_i$  reaches the threshold value  $-55$  mV, neuron  $i$  emits a spike, and then  $V_i$  is reset to  $-58$  mV. The parameter  $g$  denotes the maximal synaptic conductance. The synaptic strength  $S_j(t)$  at thalamocortical system is subjected to the STD mechanism,

$$\frac{dS_j}{dt} = \frac{1}{\tau_s} (1 - S_j) - (1 - f) S_j \delta(t - t_{sp}^j). \quad (2)$$

The parameter  $f$  ( $0.0 < f < 1.0$ ) determines the amount of depression at synapse  $j$  induced by each spike in neuron  $j$ . The parameter  $\tau_s$  denotes the depression recovery time. When the afferent neuron  $j$  fires a Poisson spike train at rate  $R_j$ , the synaptic strength will quickly decrease to the approximate steady state (SS, for a high rate  $R_j$ )<sup>24</sup>,

$$S_j(SS) = \frac{1}{f + (1-f)\tau_S R_j} \approx \frac{1}{(1-f)\tau_S R_j}. \quad (3)$$

But, for a small firing rate  $R_j$ , the synaptic strength approximately maintains its original value 1. This depression model gives a good fit of experimental data<sup>24</sup>. In the following simulations, we take  $f = 0.75$  and  $\tau_S = 200$  ms (except for parameter values in Fig. 8(a,b) for comparison), which lie within the range indicated in the experimental data<sup>26,27</sup>. The main qualitative results do not depend on the two parameters.

Experimentally, microsaccades are very fast movements<sup>3</sup>. In Ref. 17, we have studied the effect of finite microsaccadic speed and compared to experimental observations<sup>9</sup>. For simplicity, we here ignore the time course of microsaccades. In our simulations, microsaccade is regarded as a relative displacement  $\Delta M$  of the tuning curve  $G_1$ , which happens immediately.  $N$  neurons in LGN and V1 are spread uniformly in the ranges from  $-L$  to  $L$  (shown in Fig. 1), respectively. We count the total number of spikes  $N_{sp}$  of the V1 neurons in a moving time bin  $T$  as a measure of the neural response.  $N = 1000$  (except for parameter values in Fig. 8(d) for comparison),  $L = 10$  and  $T = 50$  ms (except for parameter values in Fig. 8(e) for comparison) are given. Choosing different parameter values  $N$ ,  $L$  and  $T$ , however, does not alter the qualitative results.

## Results

In this section, our model predicts several new features of microsaccade-related neural responses which are likely testable in experiments. We first describe the dependence of microsaccade-induced neural responses on stimulus brightness, represented by the input amplitude  $A$ . Then, we study the effect of widths  $\sigma_1$  and  $\sigma_2$  of the two tuning curves  $G_1$  and  $G_2$ . Finally, we provide a significant prediction that microsaccade-related neural response complies with a property “sharper is better”, which has been observed in many contexts in neuroscience, including orientation selectivity<sup>28</sup>, perceptual learning<sup>29,30</sup> and auditory processing<sup>31</sup>. Interestingly, the property exhibits a robust power-law relationship between effectiveness of microsaccades and the width of Gaussian tuning curve  $G_1$ .

**Dependence on stimulus brightness.** As shown in Eq. (3), the depression of synapse depends on the firing rate of the presynaptic LGN neuron. The higher the firing rate, the smaller the steady strength of the synapses. The stimulus brightness of fixation dot is denoted by amplitude  $A$  of the LGN neuron firing rate  $R_j$  in our model (shown in Fig. 1). Therefore, the stimulus brightness is expected to impact strongly on the microsaccade-related responses. Here, we simulated the effect of the amplitude  $A$  on neural responses induced by microsaccades. As shown in Fig. 2(a), a response peak appears soon after microsaccade, and the value depends strongly on  $A$ . In detail, we measure the dependence of baseline of neural activity before microsaccade, peak of neural activity after microsaccade, change as the difference between peak and baseline, and effectiveness as the ratio of change to baseline. Clearly, both the response baseline and peak increase linearly with the increasing of  $A$  when clear response can be induced for  $A > 50$  (Fig. 2(b)) because the input  $R_j = A \exp^{-x_j^2/\sigma_1^2}$  from LGN neuron is proportional to  $A$ . We can write the linear relations of *Baseline*  $\approx k_1(A - 50)$  and *Peak*  $\approx k_2(A - 50) + c$ , respectively. Here  $k_1$  and  $k_2$  denote the slopes of the two linear relations, and  $c$  is the value of *peak* when  $A$  is 50. Since the peak is always larger than the baseline, there is  $k_2 > k_1 > 0$ . So, the change *Peak - Baseline*  $\approx (k_2 - k_1)(A - 50) + c$  increases roughly linearly as the increasing of  $A$  (Fig. 2(c)). But, the effectiveness *Change/Baseline*  $\approx \frac{c}{k_1(A - 50)} + \frac{k_2 - k_1}{k_1}$  decreases as  $A$  becomes larger (Fig. 2(d)).

Next, we studied effect of parameter  $A$  on the saturation of microsaccade-induced neural activity. In EEG experiment data, it has been recently found that<sup>9</sup>, neural response related with microsaccade increases with the increasing of microsaccade magnitude within the small region. The increasing response reaches a saturation value for larger microsaccade magnitudes. In our simulations, the response peak increases as the microsaccade magnitude  $\Delta M$  with small size in Fig. 3. When the microsaccade magnitude increases to a threshold, the increasing response peak reaches to saturation, consistent with the experimental results in ref. 9. This saturation can be well explained as follows in our model<sup>17</sup>. When the moving distance due to large microsaccade exceeds the region with strong synapse-depression, the synaptic input will increase to the largest value ( $S_j = 1$ ) and become independent of the microsaccade magnitude, leading to saturated response. Here, we focus on effect of parameter  $A$  on the saturation. It is found that in Fig. 3, the saturation value becomes larger and larger with the increasing of  $A$ . It is because  $A$  denotes the stimulus strength of fixated dot. The large  $A$  corresponds to the large neural response  $R_j = A \exp^{-x_j^2/\sigma_1^2}$  in LGN, and so the large neural response and the responsive saturation value are produced in V1. We note that the threshold of microsaccade magnitude producing saturation is independent of  $A$ , since size of the synaptic depression region due to fixation is determined by the width of tuning curve  $G_1$  of firing  $R_j$ , which is fixed in these simulations.

**Effect of width of tuning curves.** We simulate the effect of the width  $\sigma_1$  of tuning curve  $R_j$  on microsaccade-induced neural responses in Fig. 4. It is found that, both of the response baseline and peak increase with the increasing of  $\sigma_1$  within the small region (Fig. 4(b)), because the larger  $\sigma_1$  denotes the larger inputs from LGN neurons due to the broader firing region of  $R_j$ . When the  $\sigma_1$  increases to a certain value, the microsaccade with the fixed magnitude  $\Delta M$  cannot move the fixated dot out of the depressed region of the synapses. The high response peak compared to baseline after microsaccade does not appear for the large  $\sigma_1$ , i.e. the response peak tends to the response baseline (Fig. 4(b)). So, the change *Peak - Baseline* decreases approximately to zero with the increasing of  $\sigma_1$  (Fig. 4(c)). The decreasing *Change* and the increasing *Baseline* lead to the decreasing *Effectiveness = Change/Baseline* (Fig. 4(d)).

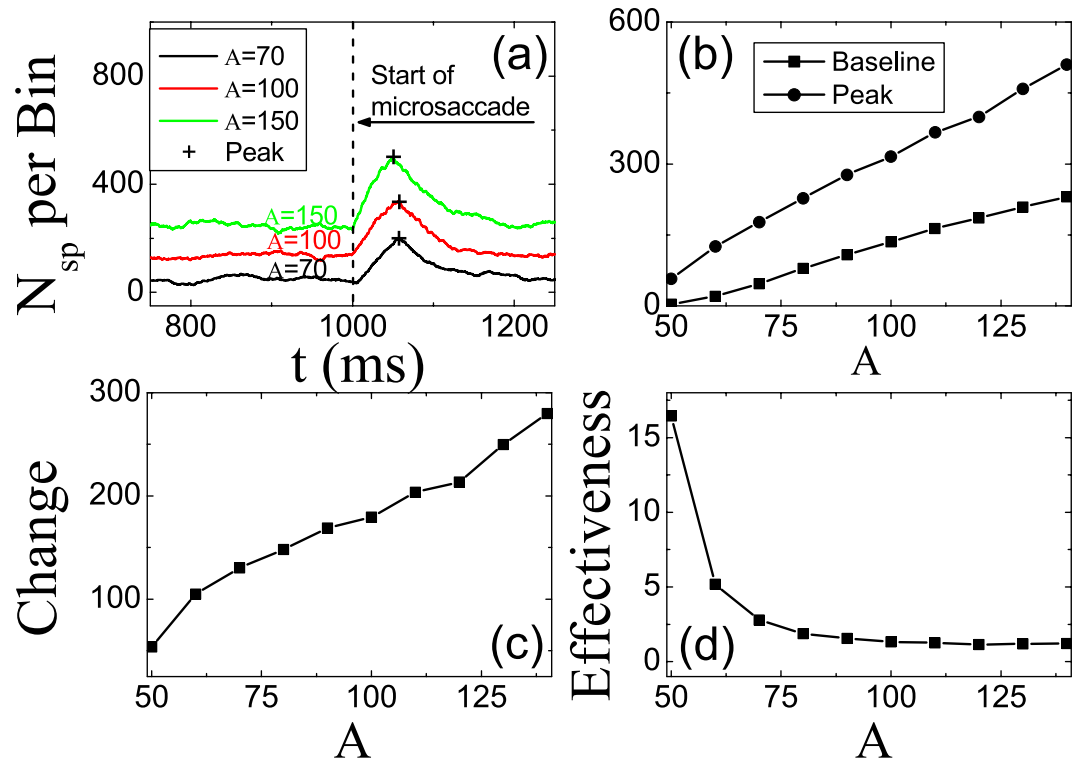


**Figure 2.** (a) Microsaccade-related neural activity for different brightness  $A$ . Microsaccade-related response baseline and peak (b), change (c) and effectiveness (d) for different brightness  $A$ . The parameters are  $g=0.15$ ,  $\Delta M=0.8$  and  $\sigma_1=\sigma_2=1.5$ . Data are averaged over 20 independent runs.

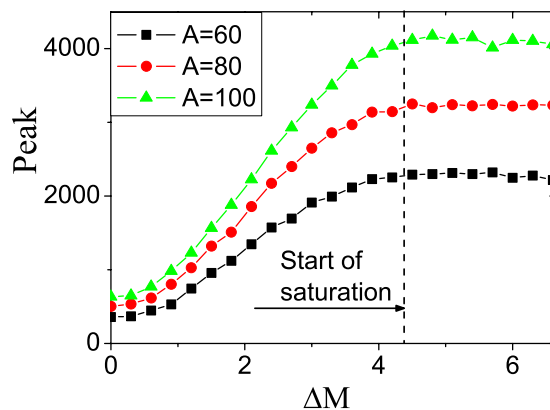


**Figure 3.** Saturation of the response peak for large microsaccades for different  $A$ . Dashed line denotes the similar threshold of microsaccade magnitude producing saturation for different  $A$ . Here  $g=0.2$ ,  $\sigma_2=1.5$  and  $\sigma_1=1.5$ . Data are averaged over 20 independent runs.

Meanwhile, we simulate the effect of the width  $\sigma_2$  of tuning curve  $W_{ij}$  on microsaccade-induced neural responses in Fig. 5. Since the larger  $\sigma_2$  reflects the larger inputs from LGN neurons due to the broader coupling region of  $W_{ij}$ , the response baseline and peak in V1 increase linearly as the increasing of  $\sigma_2$  (Fig. 5(b)). Similar to the effect of  $A$  in Fig. 2, the linear increasing of *Baseline* and *Peak* lead to the increasing of *Change* (Fig. 5(c)) and the decreasing of *Effectiveness* (Fig. 5(d)).

Next, we study effects of parameters  $\sigma_1$  and  $\sigma_2$  on the saturation of microsaccade-induced neural activity with respect to size  $\Delta M$ . As shown in Fig. 6, the saturation value becomes larger and larger with increasing  $\sigma_1$  or  $\sigma_2$ . Since the  $\sigma_1$  denotes the response region in LGN and the  $\sigma_2$  reflects the coupling region from LGN to V1, larger neural response and the responsive saturation value are produced in V1 for larger  $\sigma_1$  or  $\sigma_2$ . Particularly, a threshold of microsaccade magnitude producing the saturation depends strongly on  $\sigma_1$  (Fig. 6(a)), but not much on  $\sigma_2$  (Fig. 6(b)). With the smaller width  $\sigma_1$ , the smaller microsaccade magnitude is required for producing a saturated response. Here, we can give the following understanding. The threshold of microsaccade magnitude is

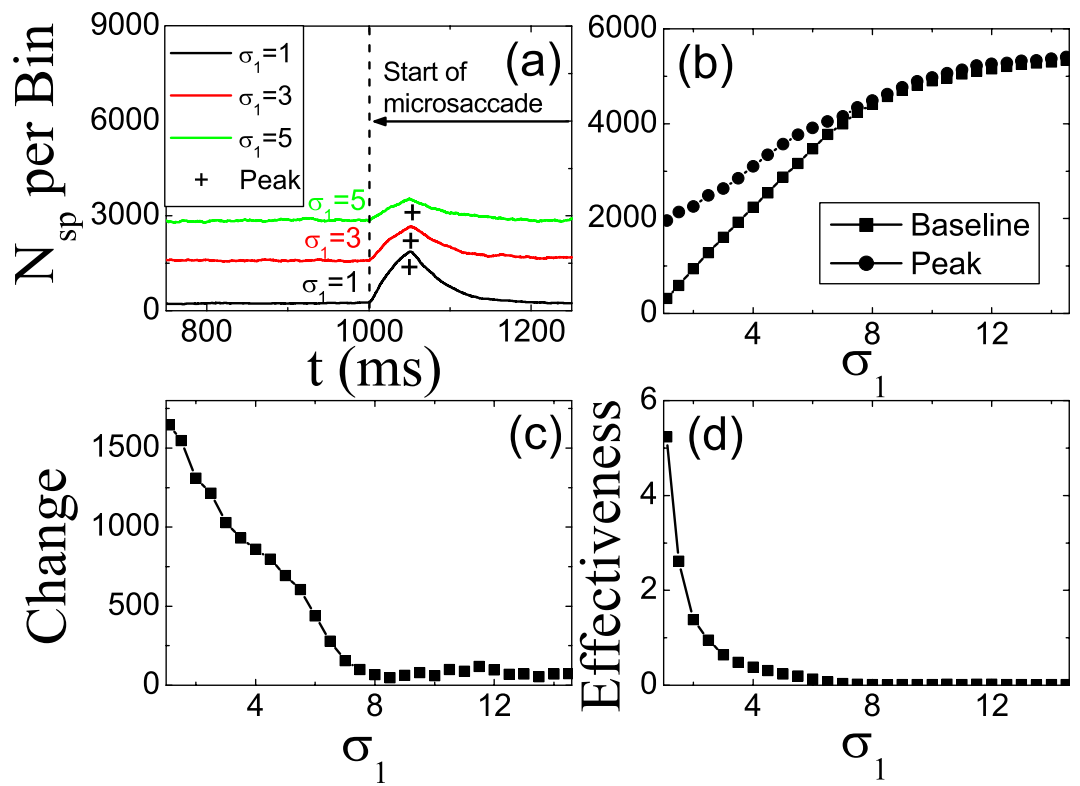


**Figure 4.** The same as in Fig. 2, but for different  $\sigma_1$ . The parameters are  $g=0.2$ ,  $A=100$ ,  $\Delta M=2.0$  and  $\sigma_2=1.5$ .

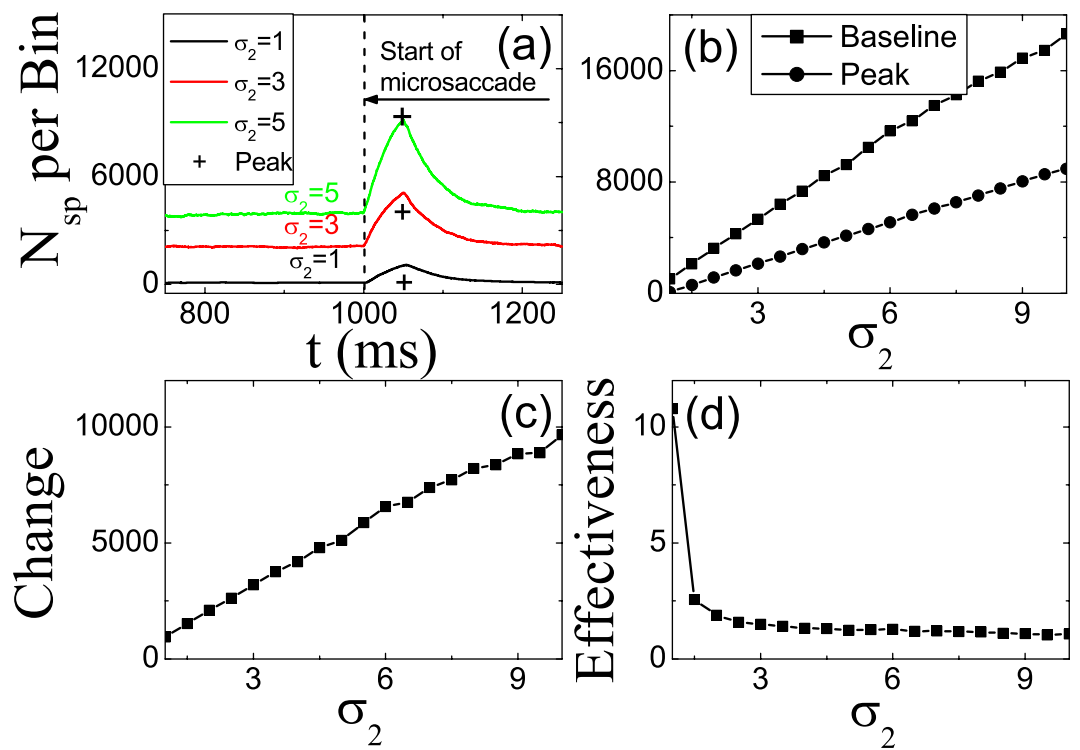


**Figure 5.** The same as in Fig. 2, but for different  $\sigma_2$ . The parameters are  $g=0.2$ ,  $A=100$ ,  $\Delta M=2.0$  and  $\sigma_1=1.5$ .

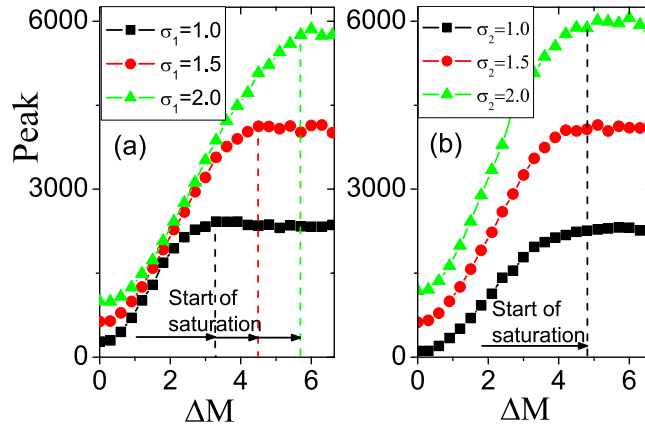


**Figure 6.** The same as in Fig. 3, but for different  $\sigma_1$  (a) and  $\sigma_2$  (b). Dashed lines denote the different thresholds of microsaccade magnitude producing saturation for different  $\sigma_1$  and  $\sigma_2$ . Here  $g = 0.2$ ,  $A = 100$ ,  $\sigma_2 = 1.5$  (a) and  $\sigma_1 = 1.5$  (b).

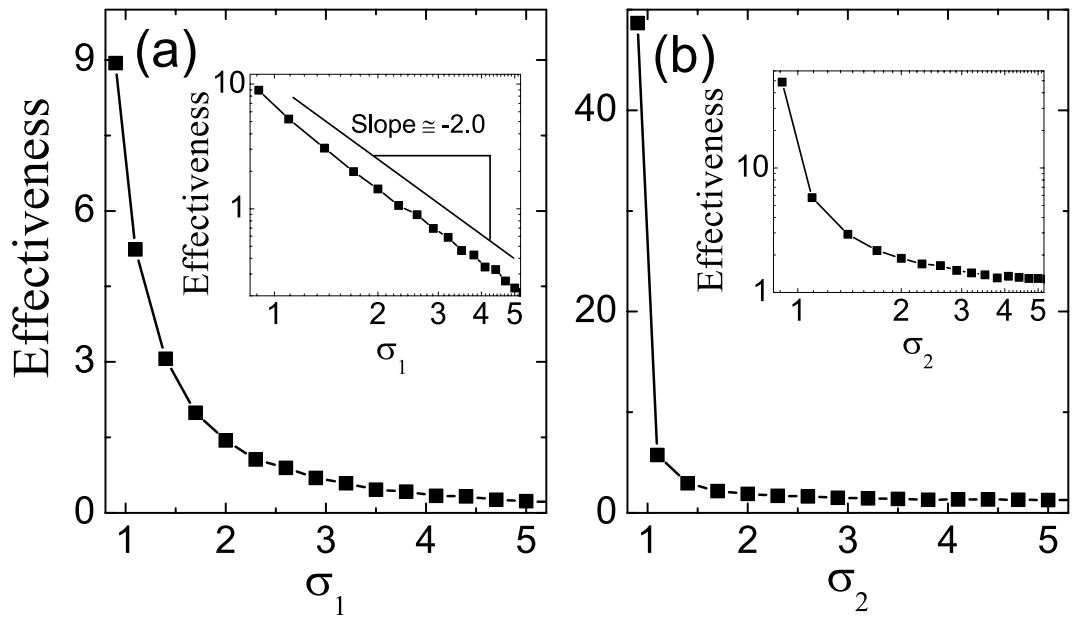


**Figure 7.** Microsaccade-related effectiveness as a function of the widths  $\sigma_1$  (a) and  $\sigma_2$  (b) of Gaussian tuning curves  $G_1$  and  $G_2$ , respectively. The insets in (a) show a power-law behavior with an exponent  $-2$  as the increase of  $\sigma_1$ . The inset in (b): similar power law does not hold for  $\sigma_2$ . The parameters are  $g = 0.2$ ,  $A = 100$ ,  $\Delta M = 2.0$ ,  $\sigma_2 = 1.5$  (a) and  $\sigma_1 = 1.5$  (b). Data are averaged over 20 independent runs.

determined by the depressed region of synapse strength  $S_j$  in space (in Eq. (3)), which strongly depends on the width  $\sigma_1$  of tuning curve  $R_j$ . The input to V1 neurons depends more strongly on the depressed region, but weakly on the width  $\sigma_2$  of tuning curve  $W_{ij}$ . The smaller the width  $\sigma_1$ , the smaller the synapse depressed region, leading to the smaller the threshold of microsaccade magnitude.

**“Sharper is better” for microsaccades.** Bell-shaped tuning curves are widely used to encode variables in the external world by many sensory and cortical neurons. Several studies have indicated that information conveyed by bell-shaped tuning curves increases as they decrease in width<sup>28–30,31</sup>. This is the so-called “sharper is better” effect. Especially, for the visual system, this has been experimentally found in many aspects of perceptual learning<sup>29,30</sup>. For example, the ability of trained monkeys to discriminate small changes is improved by sharpening of tuning curves in V1 neurons<sup>29</sup>. In our model, the microsaccade-related effectiveness reflects the relative change of neural responses after the onset of microsaccade, which supports the view: our neural system has evolved to optimally detect changes in our environment by moving eyes<sup>6</sup>. So, the effectiveness could be used to denote perceptual function. We focus on the effects of tuning curves  $G_1$  and  $G_2$  on the effectiveness. Clearly, Fig. 7 shows that microsaccade-related neural response displays the property “sharper is better”: the smaller the width ( $\sigma_1$  or  $\sigma_2$ ) of

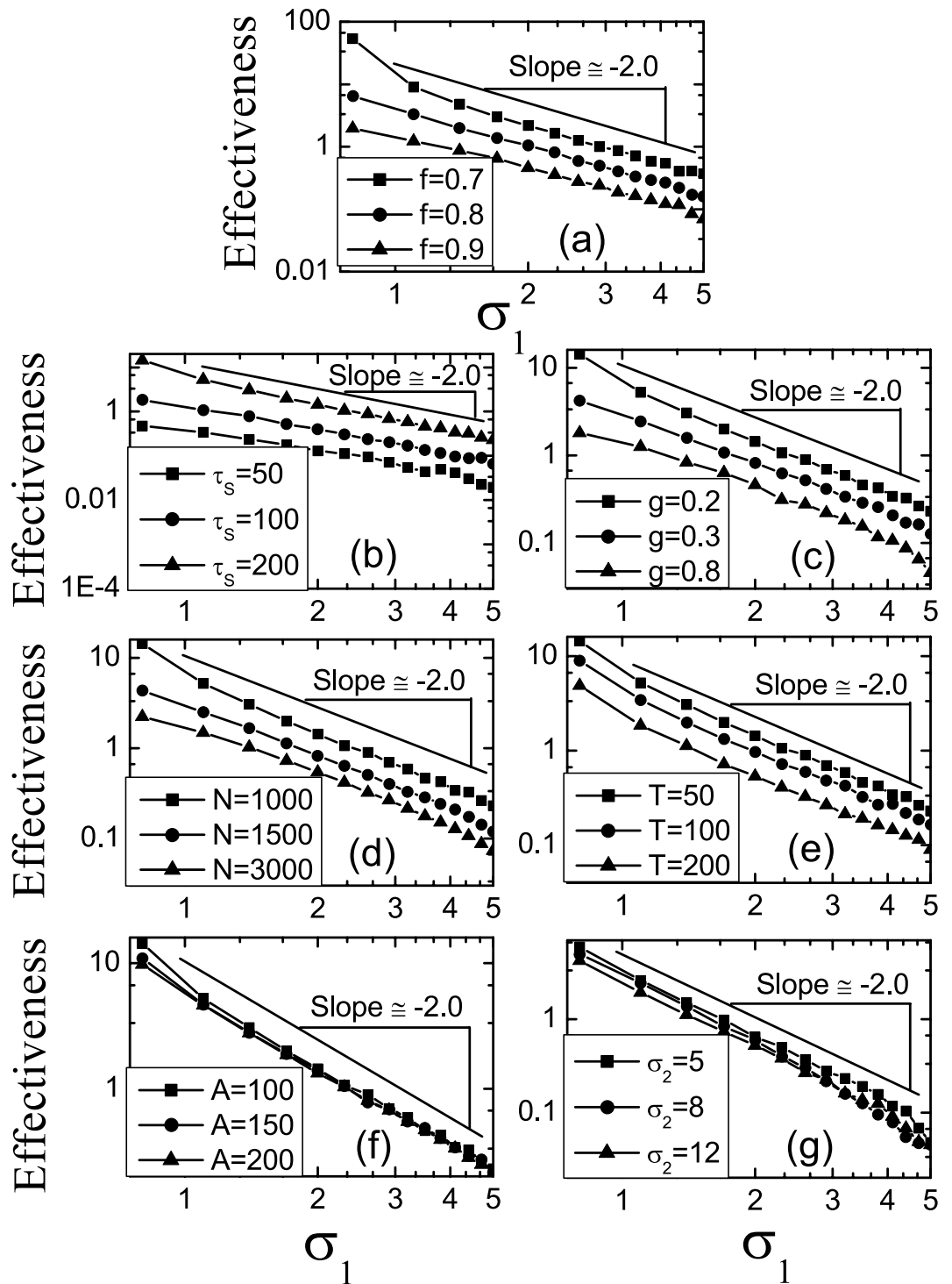


**Figure 8.** Robust power-law behavior with exponent  $-2$  as the increase of  $\sigma_1$  against some parameters,  $f$  (a),  $\tau_s$  (b),  $g$  (c),  $N$  (d),  $T$  (e),  $A$  (f) and  $\sigma_2$  (g). The parameters are  $\Delta M = 2.0$  (a–g),  $f = 0.75$  (b–g),  $\tau_s = 200$  ms (a, c–g),  $g = 0.2$  (a, b, d–g),  $N = 1000$  (a–c, e–g),  $T = 50$  ms (a–d, f, g),  $A = 100$  (a–e, g) and  $\sigma_2 = 0.15$  (a–f). Data are averaged over 20 independent runs.

the Gaussian tuning curve (i.e., the sharper the curve), the larger the effectiveness. Particularly, the microsaccade-related effectiveness exhibits a power-law property as a function of  $\sigma_1$  with an exponent  $-2$  (inset of Fig. 7(a)). A similar power law does not hold for  $\sigma_2$  (inset of Fig. 7(b)), while the effectiveness also decreases as the increasing of  $\sigma_2$ . This power-law falloff is unusual, as it implies high effectiveness of response to microsaccades for broad range of  $\sigma_1$ , indicating that this decrease is slower than exponential decay. In addition, we find that the exponent  $-2$  is quite robust against some parameters, such as  $f$ ,  $\tau_s$ ,  $g$ ,  $N$ ,  $T$ ,  $A$ ,  $\sigma_2$  and so on (Fig. 8).

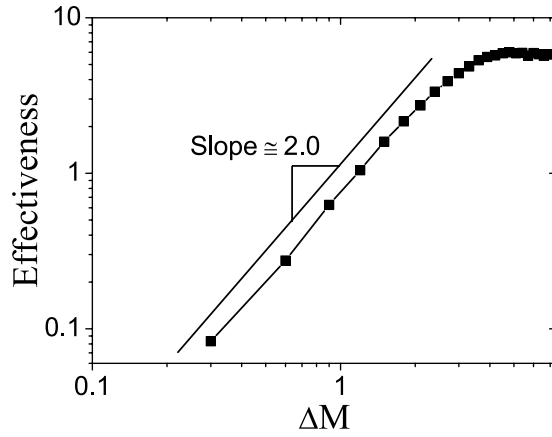


**Figure 9. Power-law property with exponent 2 as the increase of  $\Delta M$ .** The parameters are given by  $g = 0.2$ ,  $A = 100$ ,  $\sigma_1 = 1.5$  and  $\sigma_2 = 1.5$ . Data are averaged over 20 independent runs.

To explore the robust power-law property of effectiveness as a function of  $\sigma_1$ , we give the following approximate calculation. With STD of synapses, it is found that<sup>24</sup>, the total steady-state synaptic conductance resulting from a set of afferents firing at rate  $\sigma_2$  is proportional to  $R_j S_j$ . So, in the network described by Eq. (1), the V1 response baseline is proportional to the sum  $\sum_{j=1}^N R_j S_j$  of synaptical inputs from LGN before microsaccade and the V1 response peak is proportional to the sum  $\sum_{j=1}^N R'_j S_j$  after microsaccade (if we make the approximation that synapses add linearly), where  $R'_j$  denotes the firing rate in LGN after a microsaccade with small magnitude  $\Delta M$ . We let the small  $\Delta M$  not to exceed the synaptic depressed region. By using mean field theory and using the steady synapses in Eq. (3), we can get,

$$\begin{aligned}
 \text{Effectiveness} &= \frac{\text{Peak} - \text{Baseline}}{\text{Baseline}} \\
 &\propto \frac{\sum_{j=1}^N R'_j S_j - \sum_{j=1}^N R_j S_j}{\sum_{j=1}^N R_j S_j} = \frac{\sum_{j=1}^N R'_j S_j}{\sum_{j=1}^N R_j S_j} - 1 \\
 &\approx \frac{\int_{-L}^L R'_j(x) S_j(x) dx}{\int_{-L}^L R_j(x) S_j(x) dx} - 1 \\
 &\approx \frac{\int_{\Delta M - \sigma_1}^{\Delta M + \sigma_1} A e^{-\frac{(x - \Delta M)^2}{\sigma_1^2}} \frac{1}{(1-f)\tau_S A e^{-\frac{x^2}{\sigma_1^2}}} dx}{\int_{-\sigma_1}^{\sigma_1} A e^{-\frac{x^2}{\sigma_1^2}} \frac{1}{(1-f)\tau_S A e^{-\frac{x^2}{\sigma_1^2}}} dx} - 1 \\
 &\approx \frac{1}{2\sigma_1} \int_{\Delta M - \sigma_1}^{\Delta M + \sigma_1} e^{-\left[\frac{(x - \Delta M)^2}{\sigma_1^2} - \frac{x^2}{\sigma_1^2}\right]} dx - 1 \\
 &\approx \frac{\sigma_1}{4\Delta M} e^{\frac{2\Delta M x - \Delta M^2}{\sigma_1^2}} \Big|_{\Delta M - \sigma_1}^{\Delta M + \sigma_1} - 1 \\
 &= \frac{\sigma_1}{4\Delta M} \sum_{n=0}^{\infty} \frac{1}{n!} \left( \frac{2\Delta M x - \Delta M^2}{\sigma_1^2} \right)^n \Big|_{\Delta M - \sigma_1}^{\Delta M + \sigma_1} - 1 \\
 &= \frac{5}{3} \Delta M^2 \sigma_1^{-2} + 0(\sigma_1^{-2}) \\
 &\approx \frac{5}{3} \Delta M^2 \sigma_1^{-2},
 \end{aligned}$$

where  $0(\sigma_1^{-2})$  denotes higher order infinitesimal of  $\sigma_1^{-2}$  for large  $\sigma_1$ . In Fig. 7(a) and Fig. 8, the power-law relations are given for large  $\sigma_1 > 1$ . In the regime of large  $\sigma_1$ , we here focus on the relation. We can approximately get  $\text{Effectiveness} \propto \frac{5}{3} \Delta M^2 \sigma_1^{-2}$ . So, the effectiveness can be described by  $\text{Effectiveness} \approx k \left( \frac{5}{3} \Delta M^2 \sigma_1^{-2} \right) + c_0$ , where  $k$  and  $c_0$  are independent of  $\sigma_1$  and  $\Delta M$  and are determined by other parameters of V1 neural dynamics in Eqs. (1) and (2). Moreover, the effectiveness is zero for the larger  $\sigma_1$  because response peak is equal to response baseline in Fig. 4. So, the  $c_0$  is identical to 0. We finally get,



$$\text{Effectiveness} \approx \frac{5}{3}k\Delta M^2\sigma_1^{-2}. \quad (4)$$

Obviously, the effectiveness exhibits an approximate power-law form as a function of  $\sigma_1$  with a robust exponent  $-2$  irrespective of any parameters, such as  $f, \tau_s, g, N, T, A$  and  $\sigma_2$ , which is consistent with our simulations in Fig. 8. It is noted that, in the derivation of Eq. (4), the microsaccadic size  $\Delta M$  is assumed to be small enough that the microsaccade does not exceed the synaptic depressed region. The effectiveness exhibits another power-law property as a function of small  $\Delta M$  with a positive exponent 2 in Eq. (4). In our simulations, the property is verified for the microsaccade magnitudes smaller than the threshold value producing responsive saturation, shown in Fig. 9. The effectiveness maintains constant for further increasing of the large microsaccade magnitude  $\Delta M$  (shown in the right side of Fig. 9) because of the responsive saturation (see Fig. 6).

## Discussion

By using our model, we extensively study and predict the dependence of microsaccade-related neural responses and responsive saturation value on several key parameters  $A, \sigma_1$  and  $\sigma_2$ , which could be tuned in experiments. For possible verification of our theoretical predictions based on the model, we propose the following feasible experimental designs. The amplitude  $A$  and width  $\sigma_1$  of Gaussian tuning curve  $G_1$  evoked by fixated dot can be modified by changing brightness and size of the dot, which can be easily implemented in experiments. Specifically, the more brightness corresponds to the larger amplitude  $A$ , and larger dot corresponds to larger width  $\sigma_1$ . In addition, the width  $\sigma_2$  of Gaussian orientation tuning curve  $G_2$  of thalamocortical connecting weights may be modified by training certain microsaccade-related ability, motivated by ref. 29 where the orientation tuning curve at trained orientation became sharper for trained monkey, while modifications of tuning curve were not observed for the monkey which had not been trained. Then results similar to our simulations could be expected.

Particularly, the change of effectiveness due to change of  $\sigma_1$  displays strong robustness against other parameters with power-law relation. It is plausible that this property reinforces the idea that microsaccades contribute to the vision-detection function: the same microsaccade exhibits different effectiveness for different distribution width  $\sigma_1$  of light evoked by fixation dot, which seems to support the view: our neural system has evolved to optimally detect changes in our environment by moving eyes<sup>6</sup>.

In conclusion, by using a feedforward network model with STD, several new features of microsaccade-related neural responses are theoretically predicted, which could be tested in experiments. Particularly, we provide a significant prediction “sharper is better”, which has been extensively found in many aspects of perceptual learning. By using mean field theory, we give analytical study on the robust power-law property for “sharper is better”. This prediction, if experimentally verified, would strongly suggest STD in thalamocortical synapses as an important contributor to “sharper is better”. Generally, our study is the first to theoretically predict microsaccade-related neural responses by using biologically plausible model, which could be further tested in experiments. These predictions can give guidance for further experimental studies of the role of microsaccades in visual information processing. These modelling results suggest that, the depression model may be very useful for further investigating behavioral properties and functional roles of microsaccades.

## References

- Hafed, Z. M. & Clark, J. J. Microsaccades as an overt measure of covert attention shifts. *Vision Res.* **42**, 2533–2545 (2002).
- Engbert, R. & Kliegl, R. Microsaccades uncover the orientation of covert attention. *Vision Res.* **43**, 1035–1045 (2003).
- Martinez-Conde, S., Macknik, S. L. & Hubel, D. H. The role of fixational eye movements in visual perception. *Nat. Rev. Neurosci.* **5**, 229–240 (2004).
- Hafed, Z. M., Goffart, L. & Krauzlis, R. J. A neural mechanism for microsaccade generation in the primate superior colliculus. *Science* **323**, 940–943 (2009).
- Hsieh, P.-J. & Tse, P. U. Microsaccade rate varies with subjective visibility during motion-induced blindness. *PLoS One* **4**, e5163 (2009).
- Rolls, M. Microsaccades: small steps on a long way. *Vision Res.* **49**, 2415–2441 (2009).
- Martinez-Conde, S., Macknik, S. L. & Hubel, D. H. The function of bursts of spikes during visual fixation in the awake primate lateral geniculate nucleus and primary visual cortex. *Proc. Natl. Acad. Sci. USA* **99**, 13920–13925 (2002).
- Shapley, R., Hawken, M. & Xing, D. The dynamics of visual responses in the primary visual cortex. *Prog. Brain Res.* **165**, 21–32 (2007).
- Dimigen, O., Valsecchi, M., Sommer, W. & Kliegl, R. Human microsaccade-related visual brain responses. *J. Neurosci.* **29**, 12321–12331 (2009).
- Martinez-Conde, S., Macknik, S. L., Troncoso, X. G. & Dyar, T. A. Microsaccades counteract visual fading during fixation. *Neuron* **49**, 297–305 (2006).
- Martinez-Conde, S. Fixational eye movements in normal and pathological vision. *Prog. Brain Res.* **154**, 151–176 (2006).
- Tse, P. U., Baumgartner, F. J. & Greenlee, M. W. Event-related functional MRI of cortical activity evoked by microsaccades, small visually-guided saccades, and eyeblinks in human visual cortex. *NeuroImage* **49**, 805–816 (2010).
- Kagan, I., Gur, M. & Snodderly, D. M. Saccades and drifts differentially modulate neuronal activity in V1: effects of retinal image motion position and extraretinal influences. *J. Vision* **8**, 19 (2008).
- Leopold, D. A. & Logothetis, N. K. Microsaccades differentially modulate neural activity in the striate and extrastriate visual cortex. *Exp. Brain Res.* **123**, 341–345 (1998).
- Bair, W. & O’Keefe, L. P. The influence of fixational eye movements on the response of neurons in area MT of the macaque. *Vis. Neurosci.* **15**, 779–786 (1998).
- Yuval-Greenberg, S., Tomer, O., Keren, A. S., Nelken, I. & Deouell, L. Y. Transient induced gamma-band response in EEG as a manifestation of miniature saccades. *Neuron* **58**, 429–441 (2008).
- Yuan, W.-J., Dimigen, O., Sommer, W. & Zhou, C. A model of microsaccade-related neural responses induced by short-term depression in thalamocortical synapses. *Front. Comput. Neurosci.* **7**, 47 (2013).
- Levina, A., Herrmann, J. & Geisel, T. Dynamical synapses causing selforganized criticality in neural networks. *Nat. Phys.* **3**, 857–860 (2007).
- Mongillo, G., Barak, O. & Tsodyks, M. Synaptic theory of working memory. *Science* **319**, 1543–1546 (2008).

20. Boccaletti, S. *et al.* The structure and dynamics of multilayer networks. *Phys. Rep.* **544**, 1–122 (2014).
21. Abbott, L. & Regehr, W. Synaptic computation. *Nature* **431**, 796–803 (2004).
22. Tsodyks, M. & Gilbert, C. Neural networks and perceptual learning. *Nature* **431**, 775–781 (2004).
23. Poggio, T., Fahle, M. & Edelman, S. Fast perceptual learning in visual hyperacuity. *Science* **256**, 1018–1021 (1992).
24. Abbott, L. F., Varela, J. A., Sen, K. & Nelson, S. B. Synaptic depression and cortical gain control. *Science* **275**, 220–224 (1997).
25. Chance, F. S., Nelson, S. B. & Abbott, L. F. Synaptic depression and the temporal response characteristics of V1 cells. *J. Neurosci.* **18**, 4785–4799 (1998).
26. Varela, J. *et al.* A quantitative description of short-term plasticity at excitatory synapses in layer 2/3 of rat primary visual cortex. *J. Neurosci.* **17**, 7926–7940 (1997).
27. Boudreau, E. C. & Ferster, D. Short-term depression in thalamocortical synapses of cat primary visual cortex. *J. Neurosci.* **25**, 7179–7190 (2005).
28. Somers, D., Nelson, S. & Sur, M. An emergent model of orientation selectivity in cat visual cortical simple cells. *J. Neurosci.* **15**, 5448–5465 (1995).
29. Schoups, A., Vogels, R., Qian, N. & Orban, G. Practising orientation identification improves orientation coding in V1 neurons. *Nature* **412**, 549–553 (2001).
30. Yang, T. & Maunsell, J. The effect of perceptual learning on neuronal responses in monkey visual area V4. *J. Neurosci.* **24**, 1617–1626 (2004).
31. Fitzpatrick, D., Batra, R., Stanford, T. & Kuwada, S. A neuronal population code for sound localization. *Nature* **388**, 871–874 (1997).

## Acknowledgements

This work is partially supported by Hong Kong Baptist University (HKBU) Strategic Development Fund, NSFC-RGC Joint Research Scheme HKUST/NSFC/12-13/01 (or N\_HKUST 606/12), HKRGC GRF12302914, National Natural Science Foundation of China under Grant Nos. 11275027, 11005047 and 11505075, Natural Science Foundation of Anhui Province under Grant No. 1508085MA04, Great Project of Natural Science in Anhui Provincial Colleges and Universities under Grant No. KJ2015ZD33, Major Project of Outstanding Young Talent Support Program in Anhui Provincial Colleges and Universities under Grant No. gxyqZD2016410, Young Fund of Huaibei Normal University under Grant No. 2013xqz17, and Scientific and Technological Activity Foundations for Preferred Overseas Chinese Scholar in Ministry of Human Resources and Social Security of China and in Department of Human Resources and Social Security of Anhui Province.

## Author Contributions

J.F.Z., W.J.Y., Z.Z. and C.S.Z. planned the study, performed the experiments, analyzed the data, developed the theory and wrote the paper.

## Additional Information

**Competing financial interests:** The authors declare no competing financial interests.

**How to cite this article:** Zhou, J.-F. *et al.* Model predictions of features in microsaccade-related neural responses in a feedforward network with short-term synaptic depression. *Sci. Rep.* **6**, 20888; doi: 10.1038/srep20888 (2016).



This work is licensed under a Creative Commons Attribution 4.0 International License. The images or other third party material in this article are included in the article's Creative Commons license, unless indicated otherwise in the credit line; if the material is not included under the Creative Commons license, users will need to obtain permission from the license holder to reproduce the material. To view a copy of this license, visit <http://creativecommons.org/licenses/by/4.0/>